Supplementary Information

Sodium polyphosphate-induced gel interfacial layer enables a stable Zn anode under harsh conditions

Yue Shen[a], Yongkang Wang[a], Xiao Liu[a], Xingru Chen[a], Jiyu Sun[a], Beibei Yang[a]*, Qiang Huang[a]*, Yongzheng Zhang[b], Hongbin Lu[b]*, Duan Bin[a]*

[a]School of Chemistry and Chemical Engineering, Nantong University, Nantong, Jiangsu, 226019, P.R. China. E-mail: yangbeibei@ntu.edu.cn; huangqiang@ntu.edu.cn; dbin17@fudan.edu.cn

[b]School of Textile and Clothing, Nantong University, Nantong, 226019, China. luhb@nju.edu.cn

1 Experimental Section

1.1 Synthesis of SPANI cathode

Firstly, 0.728 mL of aniline and 1.38 g of 2-aminobenzene sulfonic acid were added to 40 mL of deionized water in succession, and then mixed uniformly until fully dissolved. Dissolve 3.648 g of ammonium persulfate in 40 mL of 0.1 M HCl. The two solutions are mixed and stirred continuously so that they react fully. The resulting solution was centrifuged at 5000 rpm for 30 minutes and washed with deionized water until the pH of the clarified solution reached 5. After 24 hours at room temperature, the dark green product was filtered. Finally, sulfonated polyaniline solids (SPANI) were obtained after drying in a vacuum oven at 60 ℃ for 24 hours.

1.2 Preparation of the electrolytes

To prepare a 25 mol L^{-1} $ZnCl_2$ electrolyte solution, 34.075 g of $ZnCl_2$ is added to 10 mL of deionized water, followed by the addition of 150 μL of 36% hydrochloric acid to aid dissolution. The mixture is then stirred with a magnetic stirrer until completely dissolved to obtain the $ZnCl_2$ solution.

To prepare a 0.02 g mL^{-1} SPPP solution. First, accurately weigh 0.2 g of sodium polyphosphate (SPPP) using a balance and place it into a clean beaker. Then, add a small amount of deionized water (e.g., about 5-8 mL) to the beaker. Stir gently with a glass rod until the solid is completely dissolved. Next, transfer all of the solution from the beaker into a 10 mL volumetric flask. Rinse the beaker and glass rod several times with a small amount of deionized water, and pour the rinse solution into the volumetric flask to ensure complete transfer of the solute. Finally, slowly add deionized water to the volumetric flask until the liquid level approaches the calibration mark. Use a dropper to add deionized water drop by drop until the bottom of the meniscus aligns exactly with the 10 mL mark. Seal the volumetric flask with its stopper, invert it several

times, and shake gently to ensure thorough mixing. The resulting solution is a 0.02 g mL^{-1} SPPP solution. The same method was used to obtain 0.05 g mL^{-1} SPPP, 0.5 g mL^{-1} SPPP, and 1 g mL^{-1} SPPP solutions, respectively.

1.3 Material characterization

Fourier transform infrared spectrometer (FTIR, Nicolet IS 10) in the wavenumber range of 400-2000 cm^{-1} was adopted to obtain the FTIR spectra. Raman spectra of gel material was obtained on Horiba HR32 Raman spectroscope system with laser excitation of 532 nm and wavenumber range of 400-2000 cm^{-1}. The surface morphology and chemical composition of GF and S-GF separators were characterized using a scanning electron microscope (SEM, Gemini SEM 300) and a 3D laser confocal scanning microscope (CLSM, sprint hp-opc 3000, Nanofocus). The morphology of gel material was analyzed by transmission electron microscopy (TEM). X-ray diffractometer (XRD) data for patterns were obtained with a Bruker D8 endeavor XRD, equipped with Cu Kα (λ = 0.15405 nm) radiation (40 kV, 40 mA).

1.4 Electrochemical measurement

The Zn||Zn symmetric cell was assembled in the CR2016 coin cells in an air atmosphere. Galvanostatic charge/discharge curves and long-term cycling tests were recorded on a Land CT 3002A battery-testing instrument at different current densities at room temperature. The potentiostatic current-time curves were measured on an electrochemical workstation at a fixed overpotential of -150 mV. Coulombic efficiency of Zn plating/stripping was tested at a current density of 1.0 mA cm^{-2} in the CR2016 coin cell where Cu foil serves as working electrode and Zn foil as counter electrode. The stripping cut-off voltage was set at 0.5 V vs. Zn^{2+}/Zn. The cyclic voltammetry (CV) curve and linear scanning voltammetry (LSV) were conducted using an electrochemical workstation (CHI660E). The CV of Zn plating/stripping was tested in a three-electrode cell where Ti foil serves as working electrode, Zn foil as counter and reference electrode

at 1 mV s^{-1}. The electrochemical stability window at 1 mV s^{-1} was also applied by CV under the above system. The LSV measurement was carried out at a sweep rate of 5 mV s^{-1} in a three-electrode configuration, where Ti foil, graphite rod and saturated calomel electrode (SCE) were used as working, counter, and reference electrodes, respectively. The formula for EDLC is C = i/v (C: capacitance, i:current，v: sweep rate), where I is defined as half the difference between the positive and negative scan currents at each scan rate. Tafel plots were measured at a voltage range from -0.2 to 0.2 V (vs. Zn^{2+}/Zn) in Zn||Zn symmetric cells with a scan rate of 1 mV s^{-1} and then managed for linear fitting. The EIS spectras (from 100 kHz to 0.1 Hz) were tasted on an electrochemical workstation (Bio-Logic SP-200). The data and calculation process related to the DOD are acquired from the followed equations:

$$DOD\ (\%) = \frac{Cactual}{Ctheoretical} \times 100\% = \frac{I \times t \times S}{m \times Ctheoretical} \times 100\%$$

Where Cactual (mAh g^{-1}) is actual specific capacity of deposited/stripped Zn, Ctheoretical (mAh g^{-1}) is theoretical specific capacity of Zn anode (~820 mAh g^{-1}), I (mA cm^{-2}) is the current density during plating/stripping process, t (h) is the deposited/stripped time of Zn, S (cm^2) and m (g) are actual area and mass of electrode, respectively. Specifically, the depth of discharge at the current densities of 5 mA cm^{-2} (5 mAh cm^{-2}) and 10 mA cm^{-2} (10 mAh cm^{-2}):

$$DOD\ (89.5\%) = \frac{10\ mA\ cm-2 \times 1\ h \times 1.13\ cm2}{0.077\ g \times 820\ mAh\ g-1} \times 100\% = 89.5\%$$

1.5 Fabrication of Zn||PTO full cell

Electrochemical characterization of the Zn||SPANI full cell was performed using both CR2016 coin cells. The cathode material was fabricated by mixing the active material (SPANI), Ketjen Black (KB), and PTFE (binder) at a mass ratio of 6:3:1. The cathode material was rolled into a thin sheet, cut into 10 mm pellets, and pressed onto

a titanium sheet (12 mm) with approximately 2-3 mg of active materials. Full cells were assembled in CR2016 coin cells under an air atmosphere, with Zn foil (100 μm thickness) as the anode and a glass fiber filter (Whatman, GF/C) as the separator. After fine sanding with 1200 grit sandpaper to remove surface oxides, wipe the surface with alcohol and leave to dry. Then 12 mm diameter discs were cut to be used as Zn negative electrodes for button cell assembly. The tests related to the Zn||SPANI full cell were performed on a Land CT 3002A and CHI660E. The full cells were cycled in a potential range of 0.4 and 1.6 V vs. Zn^{2+}/Zn.

1.6 Ionic Conductivities of Electrolytes

The ionic conductivity of SPPP solutions at different concentrations were measured using a Bio-Logic SP-200 electrochemical workstation. The ionic conductivity of five SPPP solutions was investigated at 25 °C using the electrochemical impedance spectroscopy (EIS) technique. Two parallel Ti plate electrodes (1 cm × 1.2 cm) were used as electrodes. The measurements were conducted within a frequency range of 0.1 to 105 Hz. The conductivity values were calculated using the following equation.

$$\sigma = \frac{l}{A \times R\Omega}$$

Where σ represents the ionic conductivity of electrolyte (S cm^{-1}), l represents the electrode spacing (cm), A represents the contact area between the electrode and the electrolyte (cm^2), and R_Ω denotes the ohmic resistance.

1.7 Computational details

The binding energy calculations were conducted utilizing the Gaussian 09 W software. The molecular structures were optimized using the wB97XD functional and 6-31G(d) basis set to correct van der Waals forces. The same theoretical were employed to analysis vibrations, ensuring that the optimized structural energy is minimized. The dielectric constant (ε) was set to 78.35 to consider the solvation effect of water.

The binding energy (E_b) between Zn^{2+} and H2O solvent or SPPP molecule is defined as follows:

$$E_b = E(\mathrm{A/Zn^{2+}}) - E(A) - E(\mathrm{Zn^{2+}})$$

where $E(A/Zn^{2+})$ is the total energy of Zn^{2+} and H_2O or SPPP Combined system, and E(A) is the energy of H_2O or SPPP molecule.

Finite element simulations were performed using COMSOL Multiphysics 6.2, in which the Tertiary Current Distribution physics interface was employed to model the electric field and ionic concentration fields. The ion concentration was governed by Fick's first law of diffusion, while ion migration followed the Nernst–Planck equation.

$$\frac{\partial c_i}{\partial t} = \nabla \bullet \left(D_i \nabla c_i + z_i u_{m,j} F c_i \nabla_{\varphi} \right)$$

$$u_{m,j} = \frac{D_i}{RT}$$

Where the c_i denotes the electrolyte ion concentration, t is time, D_i represents the diffusion coefficient of different ionic species in the electrolyte, z_i is the charge number of each ionic species, $\mu_{m,j}$ is the ionic mobility, F is the Faraday constant, η is the overpotential, R is the gas constant, and T is the absolute temperature.

Both models consider a simplified geometry of the research domain. The two electrodes have a length of 10 μm and are separated by a distance of 7 μm. Multiple deposition sites are uniformly distributed on the negative electrode. The separator structure is simplified based on its actual morphology, and the primary simulation domain focuses on the electrode–separator interface. For the boundary conditions, the positive electrode is set as a zero-potential boundary, while the potential of the negative electrode is defined by the cell polarization voltage. The initial Zn^{2+} concentration is set to 2 M. The diffusion coefficient of Zn^{2+} in the electrolyte is assigned values of 2×10^{-15} m^2 s^{-1} and 5×10^{-15} m^2 s^{-1}, respectively. The exchange current density of the cell is set to 1 mA cm^{-2}, and the system temperature is fixed at 298 K.

1.8 Measured process of the wettability

The contact angle is a key parameter for characterizing surface wettability, and its

measurement must follow a precise operational procedure to ensure the accuracy and repeatability of the results. Prior to testing, the solid substrate must undergo rigorous treatment: the separator is sequentially cleaned via methods such as ultrasonic cleaning (e.g., using acetone, ethanol, and deionized water) or plasma treatment to remove organic contaminants and static electricity, followed by drying in a clean environment. The most commonly used test liquid is ultrapure water (resistivity > 18.2 MΩ·cm).

To minimize errors, measurements must be performed under controlled conditions. The test should be conducted at an ambient temperature of 20–25°C and a relative humidity of 40–60%. The instrument should be placed on a vibration-free table in a low-dust environment to prevent contamination of the sample or the droplet. During the specific measurement, the prepared sample is placed horizontally on a leveled stage. A blunt needle (outer diameter ~0.5 mm) connected to a clean micro-syringe is positioned 1–2 mm above the sample surface. Then, 2–5 μL of ultrapure water is slowly dispensed, either by allowing it to drop naturally from the needle tip or by using the more precise "needle-in" method, where the droplet is brought into contact with the surface before lowering the stage to deposit it. After an equilibration period of 3–10 seconds, a clear, high-contrast side-view image of the static sessile droplet is captured. The contact angle is subsequently calculated via software analysis; the most accurate method involves fitting the entire droplet profile to the Young-Laplace equation, which corrects for gravitational distortion. The left and right contact angles are calculated and averaged. The above steps are repeated at least five different locations on the sample surface, and the average value and standard deviation are calculated, ultimately yielding the contact angle of the separator.

2. Supplementary Figures

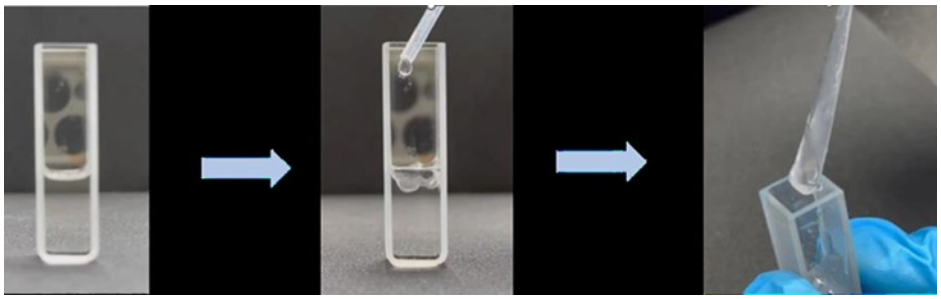

Figure S1. The formation process of SPPP-induced gel.

Note to Figure S1:

The S-GF separators were fabricated by infiltrating pristine GF separators with SPPP solutions of varying concentrations.

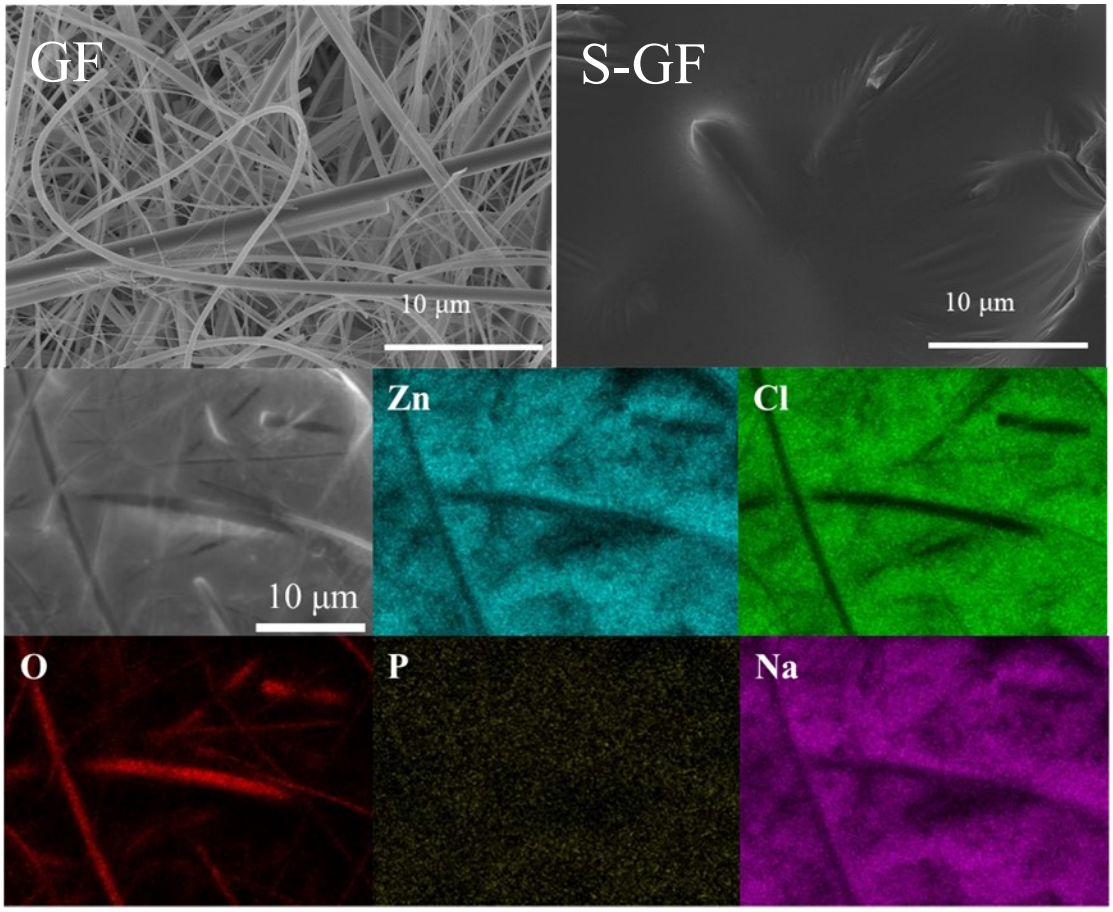

Figure S2. TEM images of GF and S-GF separators and the EDX spectrum of S-GF separator.

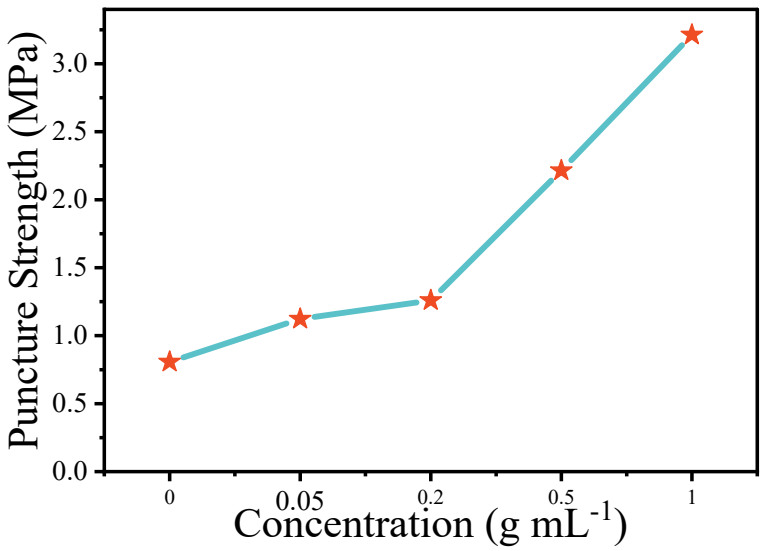

Figure S3. The puncture stress test of S-GF separator at different concentrations.

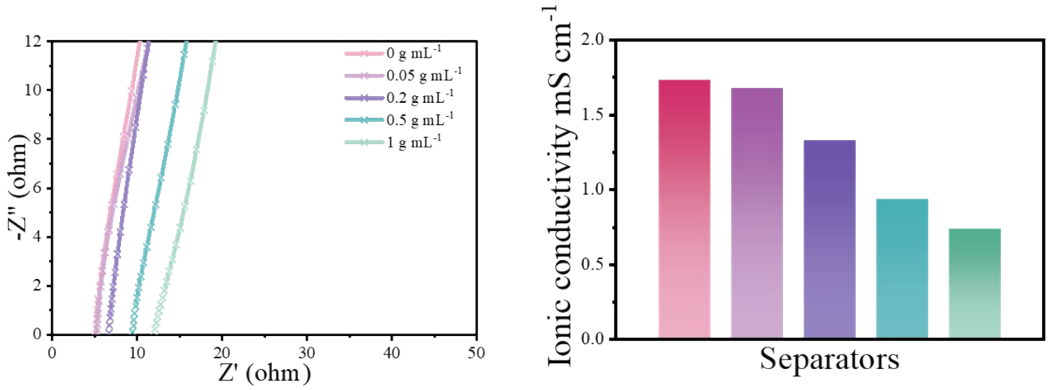

Figure S4. Ionic Conductivity of S-GF separator at different concentrations.

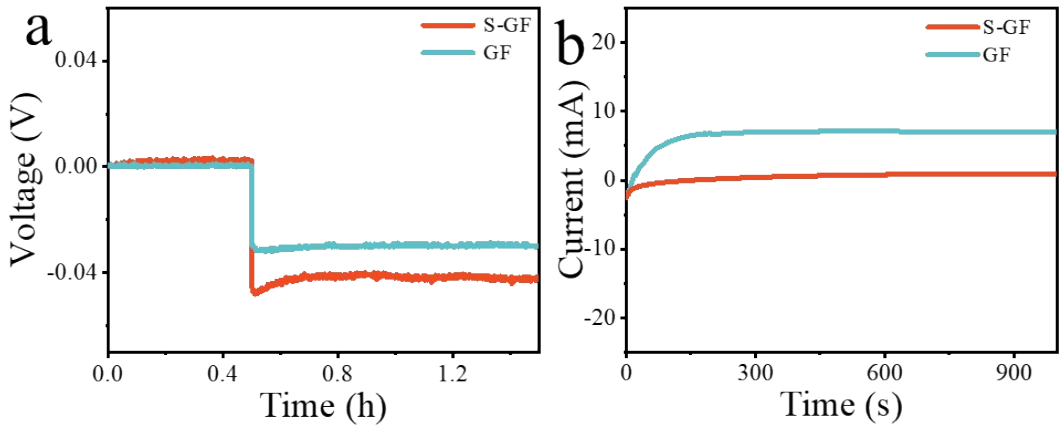

Figure S5. (a) Nucleation overpotentials of Zn deposition on GF and S-GF separators in asymmetric batteries, (b) CA profiles of GF and S-GF separator.

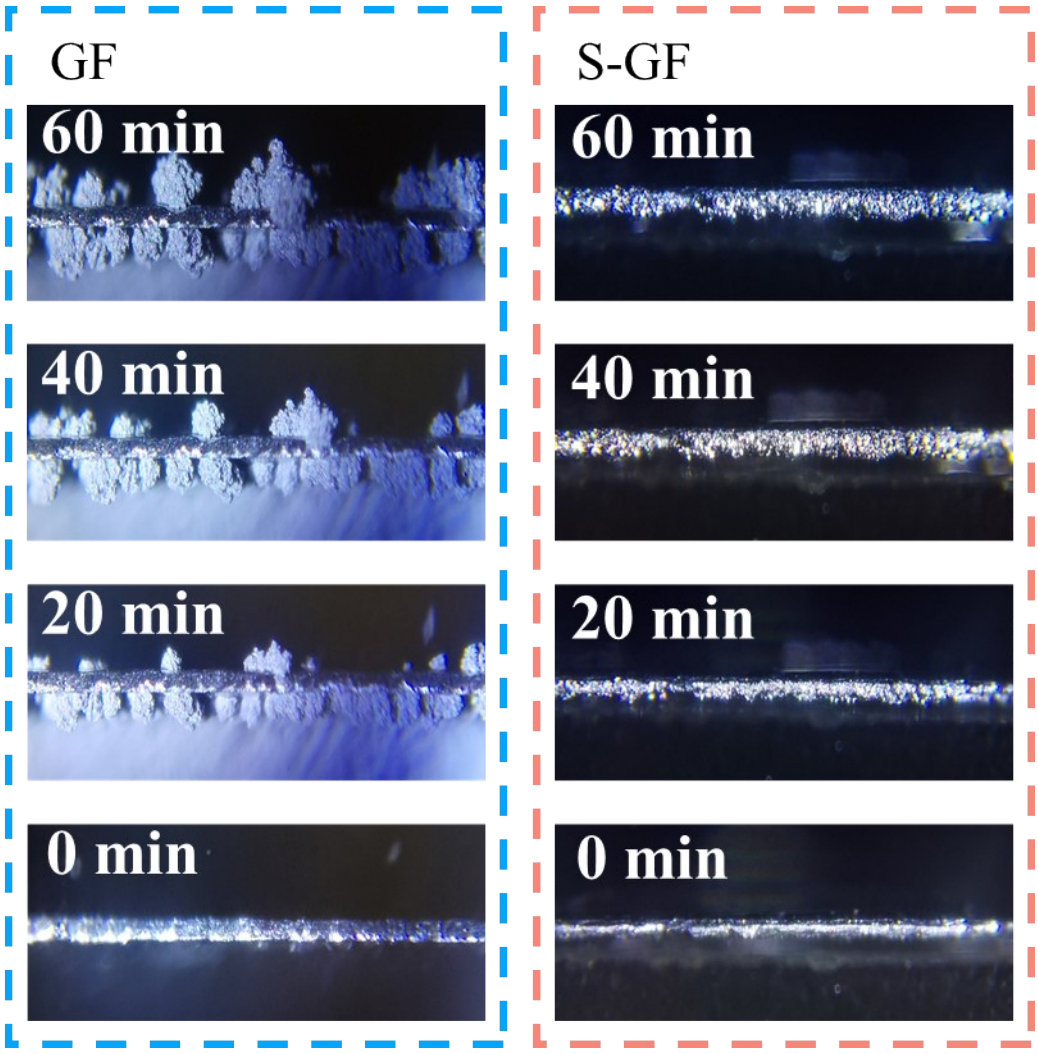

Figure S6. In-situ optical images of interfacial evolution on GF and S-GF separators during electrochemical cycling.

Note to Figure S2:

Real-time imaging revealed distinct interfacial behaviors during zinc deposition. The GF separator exhibited sharp protrusions and abundant bubble nucleation, indicating significant gas evolution and inhomogeneous zinc growth. In contrast, the S-GF separator maintained a smooth surface with no visible dendrites or bubbles, demonstrating stable, compact zinc deposition.

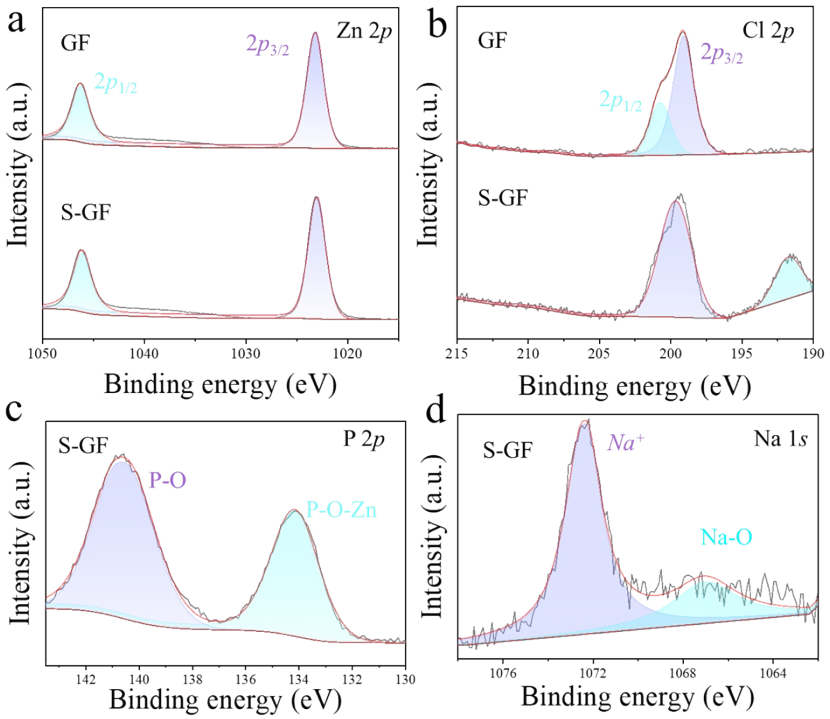

Figure S7. XPS spectrum analysis of Zn anode after 50 cycles for (a) Zn 2p, (b) Cl 2p, and (c) P 2p, (d) Na 1s.

Note to Figure S4:

Fig. S7a shows both GF and S-GF exhibit peaks for Zn $2p_{1/2}$ and Zn $2p_{3/2}$, demonstrating the presence of metallic zinc in both separators. **In Fig. S7**b, GF exhibits a single characteristic peak at ~198 eV, which corresponds to the Cl^- from the $ZnCl_2$ in the electrolyte. For S-GF, its Cl 2p spectrum still retains the Cl^- peak associated with $ZnCl_2$, while a new characteristic peak appears at ~ 192 eV corresponding to free Cl^- ions. This change directly confirms the successful introduction of Na^+ during the modification process, causing some Cl^- ions to dissociate from their strong complexation with Zn^{2+}, resulting in a state closer to that of free ions. As shown in **Fig. S7**c, the main peak located at a binding energy of approximately 133.4 eV is attributed to the P-O-Zn bond. This arises from the coordination of Zn^{2+} with the oxygen atoms in the polyphosphate (PO_4^{3-}) groups, forming Zn-O-P coordination bonds. Another shoulder peak at a binding energy of about 140.2 eV can be assigned to the P-O bond in the phosphate groups, originating from PO_4^{3-} groups that are not fully coordinated. **In Fig. S7**d, the single peak at 1071.2 eV is the typical binding energy for Na^+,

confirming the presence of Na^+ in the modified material. Its source is precisely the SPPP introduced during the preparation process.

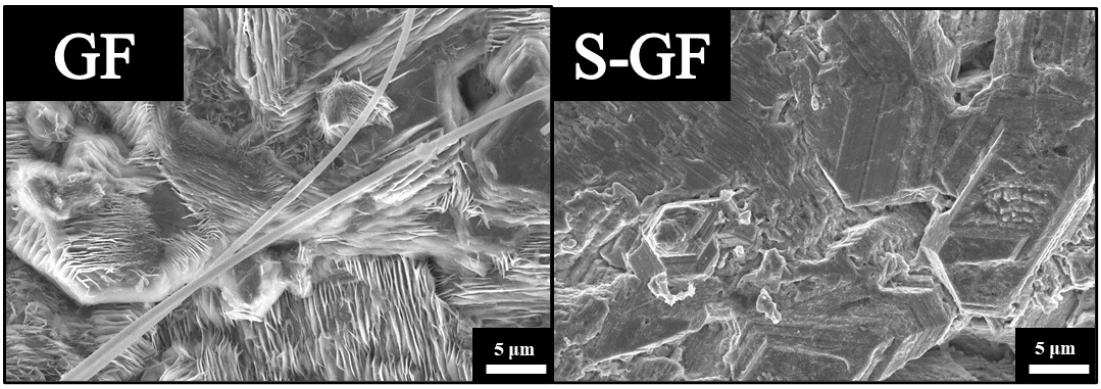

Figure S8. SEM images of Zn anode after 50 cycles under the capacity of 1 mAh cm^{-2} and current density of 1 mA cm^{-2}.

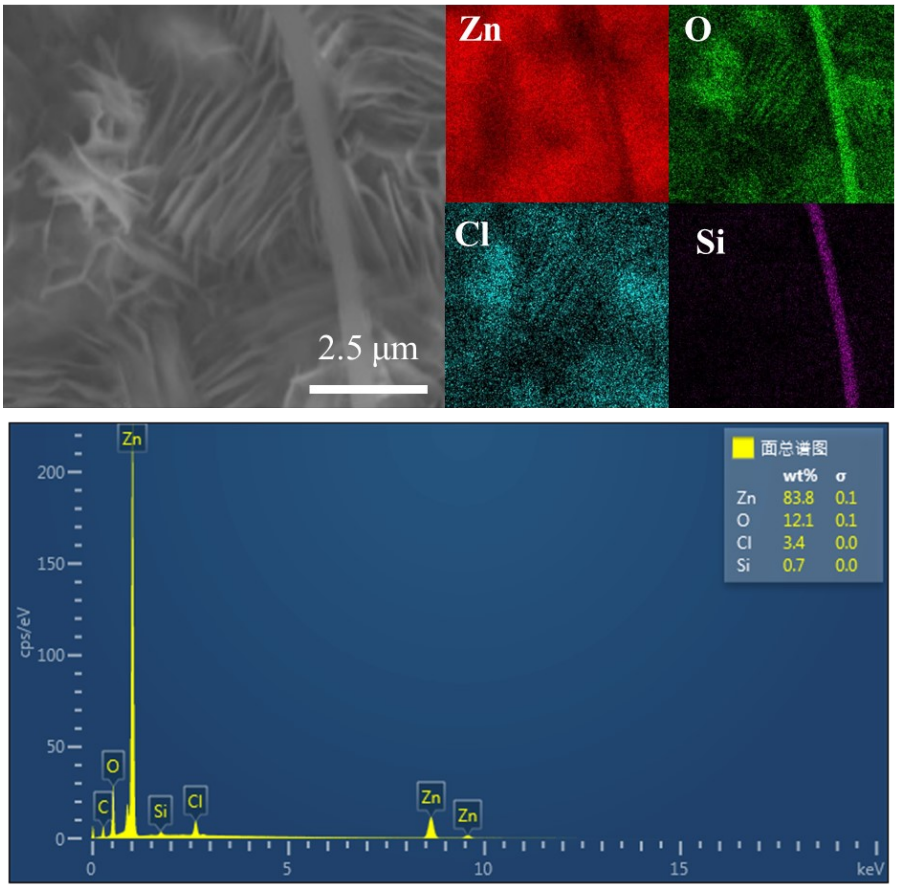

Figure S9. The corresponding EDS mapping of Zn anode with the GF separator after 50 cycles under the capacity of 1 mAh cm^{-2} and current density of 1 mA cm^{-2} and elemental composition of Zn anode surface.

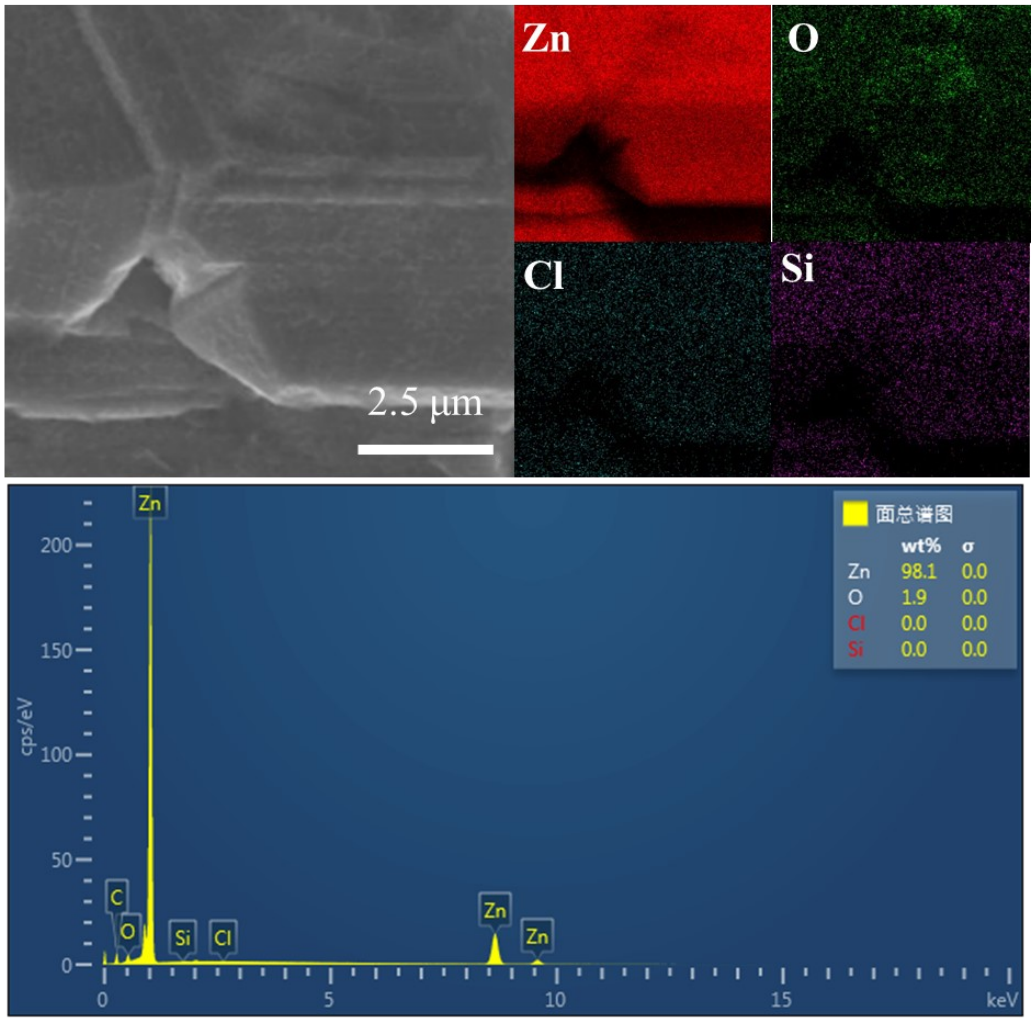

Figure S10. The corresponding EDS mapping of Zn anode with the S-GF separator after 50 cycles under the capacity of 1 mAh cm^{-2} and current density of 1 mA cm^{-2} and elemental composition of Zn anode surface.

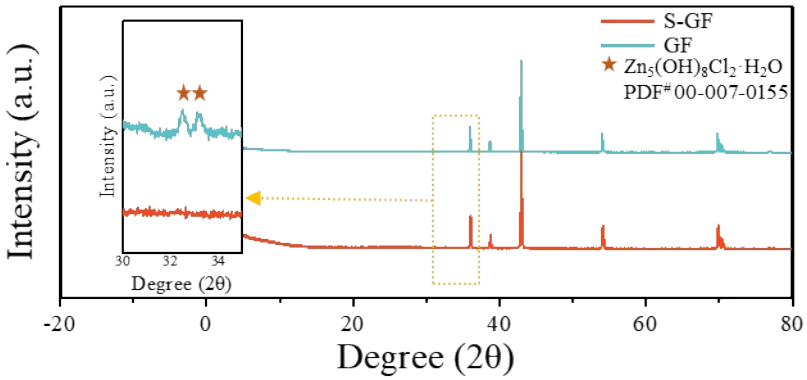

Figure S11. XRD patterns of Zn anode using GF and S-GF separators.

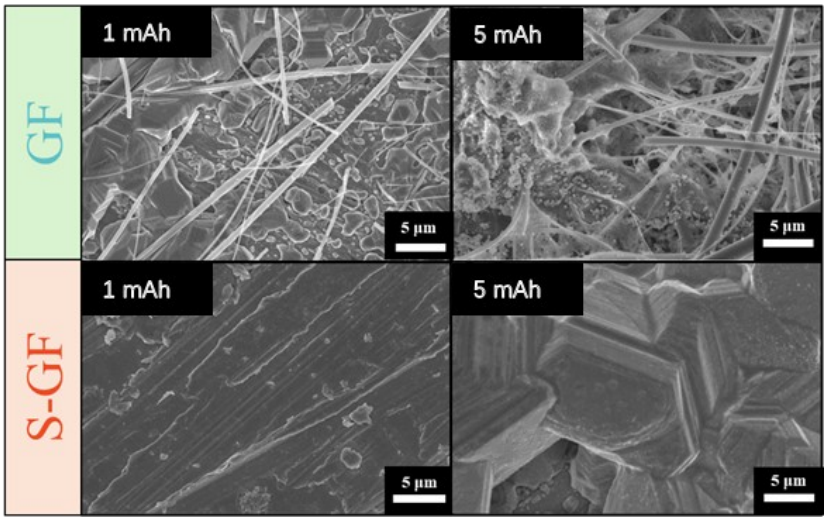

Figure S12. S-GF and GF separators generate thermal signals under a NIR laser captured by a thermometer.

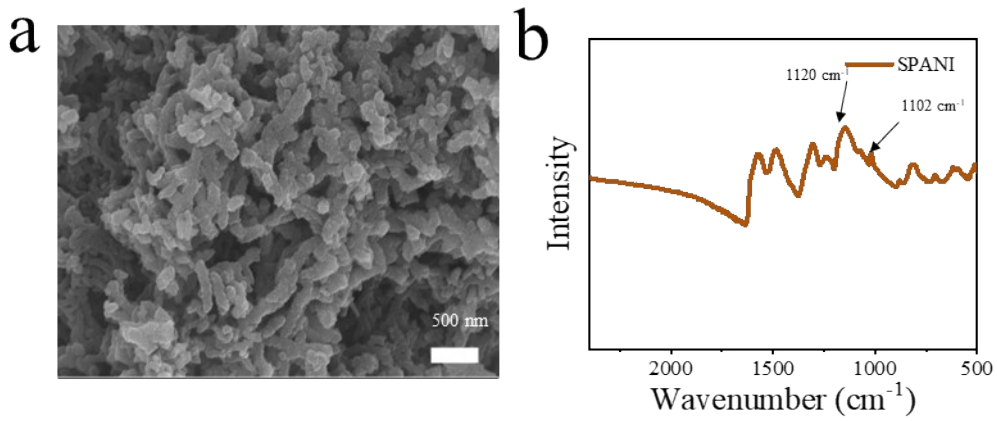

Figure S13. TEM image and FTIR spectra of the SPANI.

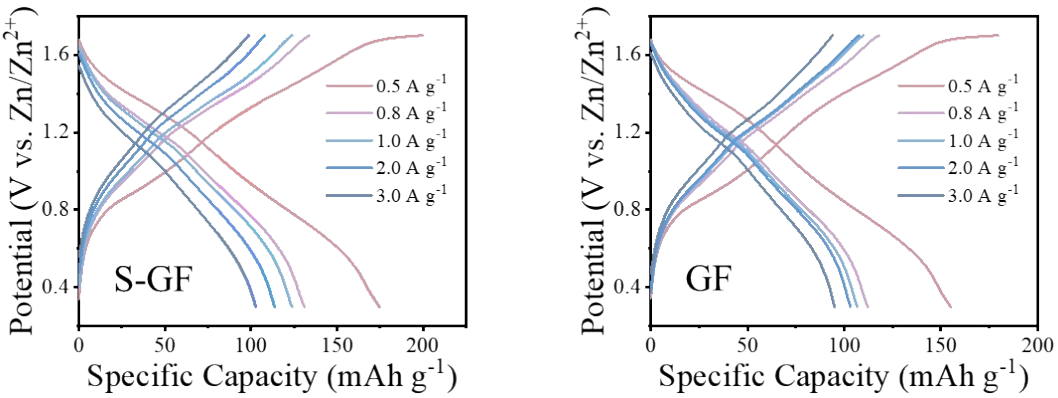

Figure S14. Charge/discharge profiles of Zn||SPANI cells assembled with GF and S-GF separators at different current densities.

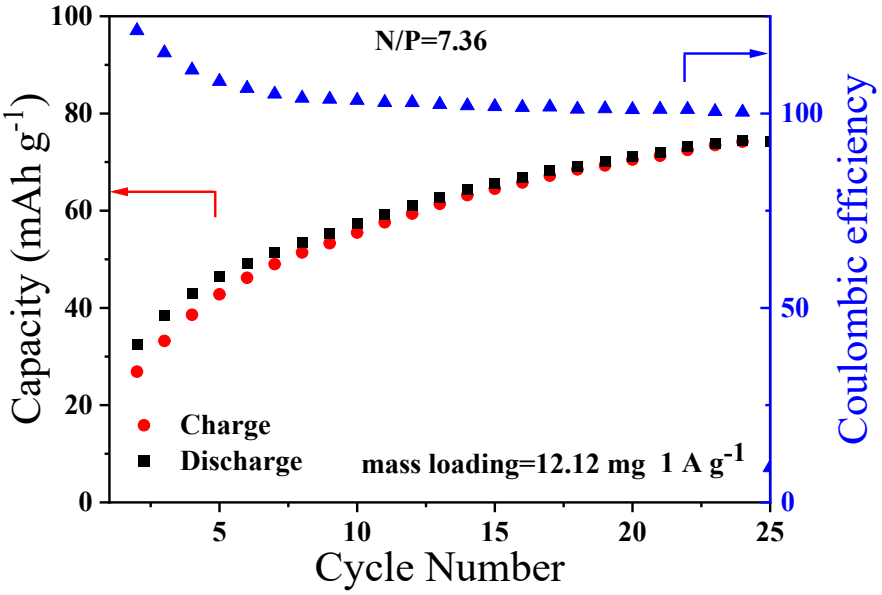

Figure S15. Cycling performance of Zn||SPANI full batteries assembled with S-GF cycling stability at 1 A g^{-1}.

Note to Figure S16:

The full-cell was cycled for 25 cycles, with a cathode areal loading is 10.73 mg cm^{-2}, delivering a corresponding areal capacity of 0.795 mAh cm^{-2}. The Zn anode exhibits the capacity ratio (N/P) of 7.36. The electrolyte amount is 400-500 µL.

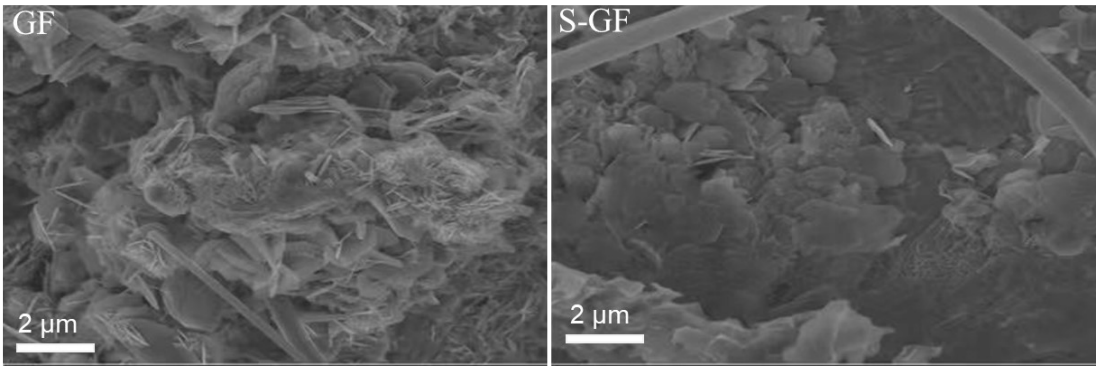

Figure S16. SEM images of Zn anodes deposited after 100 cycles of charging-discharging for Zn||SPANI full batteries.

Table S1 Different Zn anode modification methods and the corresponding electrochemistry performance.

Journal	DOD (%)	Lifespan (h)	Ref.
★	89.5	2100	This work
Angew. Chem. Int. Ed.	85	800	1
Adv. Energy Mater.	80.9	100	2
Nat. Commun.	85.6	600	3
Angew. Chem. Int. Ed.	80	280	4
Adv. Energy Mater.	68.3	130	5
Adv. Funct. Mater.	81	110	6
Angew. Chem. Int. Ed.	80	250	7
Adv. Energy Mater.	77	1000	8
Angew. Chem. Int. Ed.	50	200	9
Adv. Funct. Mater	67	300	10

3. Supplementary Reference:

1 H. Yao, Y. Li, Z. Chen, J. Chen, C. Du, Y. Chen, J. Chen, M. W. Wong, J. Zhao and D. Yuan, *Angew Chem. Int. Ed.*, 2024, **63**, e202411056.

2 W. Zhang, F. Guo, H. Mi, Z. Wu, C. Ji, C. Yang and J. Qiu, *Adv. Energy Mater.*, 2022, **12**, 2202219.

3 C. Yang, P. Woottapanit, S. Geng, R. Chanajaree, Y. Shen, K. Lolupiman, W. Limphirat, T. Pakornchote, T. Bovornratanaraks, X. Zhang, J. Qin and Y. Huang, *Nat. Commun*, 2025, **16**, 183.

4 Q. Zhang, J. Luan, L. Fu, S. Wu, Y. Tang, X. Ji and H. Wang, *Angewandte Chemie*, 2019, **131**, 15988–15994.

5 Y. Chen, S. Zhou, J. Li, J. Kang, S. Lin, C. Han, H. Duan, S. Liang and A. Pan, *Adv. Energy Mater.*, 2024, **14**, 2400398.

6 P. Cao, X. Zhou, A. Wei, Q. Meng, H. Ye, W. Liu, J. Tang and J. Yang, *Adv. Funct. Mater.*, 2021, **31**, 2100398.

7 J. Yu, Z. Song, Q. Qi, X. Hui, Y. Ma, F. Chen, K. Qi, Q. Meng, R. Li, L. Zhuang, K. Cheung Chan, Z. Chen, B. Y. Xia and Z. Xu, *Angew Chem. Int. Ed.*, 2025, **64**, e202423236.

8 H. Yan, S. Li, Y. Nan, S. Yang and B. Li, *Adv. Energy Mater.*, 2021, **11**, 2100186.

9 P. X. Sun, Z. Cao, Y. X. Zeng, W. W. Xie, N. W. Li, D. Luan, S. Yang, L. Yu and X. W. (David) Lou, *Angew Chem. Int. Ed.*, 2022, **61**, e202115649.

10 F. Duan, X. Yin, J. Ba, J. Li, Y. Yu, C. Wang, Y. Wei and Y. Wang, *Adv. Funct. Mater.*, 2024, **34**, 2310342.